Article

Dynamical Flexibility and Proton Transfer in the Arginase Active Site Probed by ab Initio Molecular Dynamics

Ivaylo Ivanov, and Michael L. Klein

J. Am. Chem. Soc., **2005**, 127 (11), 4010-4020• DOI: 10.1021/ja043693i • Publication Date (Web): 25 February 2005

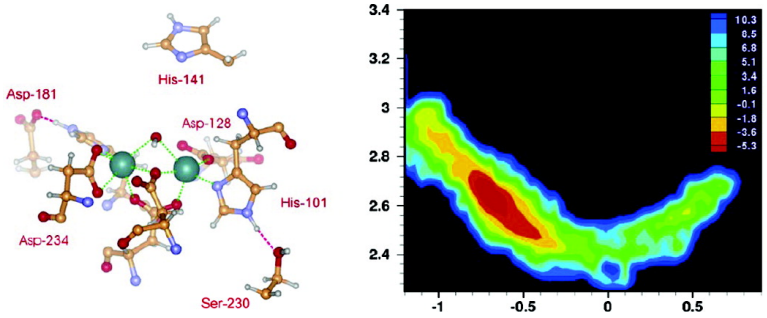

More About This Article

Additional resources and features associated with this article are available within the HTML version:

- Supporting Information
- Links to the 1 articles that cite this article, as of the time of this article download
- Access to high resolution figures
- Links to articles and content related to this article
- Copyright permission to reproduce figures and/or text from this article

View the Full Text HTML

J|A|C|S
ARTICLES
Published on Web 02/25/2005

Dynamical Flexibility and Proton Transfer in the Arginase Active Site Probed by ab Initio Molecular Dynamics

Ivaylo Ivanov* and Michael L. Klein

Contribution from the Center for Molecular Modeling and Department of Chemistry, University of Pennsylvania, 231 South 34th Street, Philadelphia, Pennsylvania 19104-6323

Received October 16, 2004; E-mail: iivanov@cmm.chem.upenn.edu

Abstract: We have used ab initio molecular dynamics (AIMD) to investigate the dynamical flexibility of the bridged binuclear structural motif in the active site of arginase. Dynamical transformations play a crucial role in catalysis. We have provided direct insight into the motions of the first-shell ligands with emphasis on the chelating and bridging carboxylates. In the case of the terminal Asp234 residue we observe changes in the binding mode (carboxylate shifts). AIMD dynamics of sufficient duration has allowed us to observe proton transfer from the bridging nucleophile to the catalytically essential Asp 128 residue and to map the underlying free energy surface in terms of simple reaction coordinates, such as the oxygen−oxygen distance R_{o-o} and the asymmetric stretch δ. This has provided valuable insight into the nature of the last step of the catalytic cycle. In addition, constrained molecular dynamics permitted us to compare the deprotonation free energy of the bridging nucleophile in the case of native versus metal-depleted arginase.

1. Introduction

Many enzymes have evolved to include well-defined constellations of metal ions in their active sites and utilize these metal clusters to catalyze a vast array of chemical transformations.[1−4] Often, seemingly identical structural motifs are used by different enzymes to carry out different reactions. It is intriguing to find out why such motifs are preferred over other possible arrangements of ligands and to unravel the subtle structural differences in the active sites of these enzymes, leading to strikingly different chemistries. Herein, we focus on a "bridged bimetal" structural motif commonly encountered in enzymes such as arginase, alkaline phosphatase, manganese catalase, ribonucleotide reductase, and various aminopeptidases.[5−11] The motif consists of two metal cations bridged by an endogenous ligand (usually a bidentate carboxylate) and one or more exogenous ligands. In addition, the two metals are quasi symmetrically coordinated, each by a histidine residue and a terminal carboxylate ligand. Some enzymes may additionally possess another mono- or bidentate bridging carboxylate ligand. Such a carboxylate-rich ligand environment presents definite advantages for redox enzymes in fine-tuning the redox potential of the metals. It is puzzling, however, that the same active site architecture should be utilized in the case of hydrolytic enzymes, where carboxylates are likely to decrease the nucleophilicity of the exogenous ligand and, hence, decrease the likelihood of a nucleophilic attack.[11] To examine these issues in detail, we selected arginase as an example of an enzyme possessing the bridged bimetal motif and studied its active site by computational means. Arginase (L-arginine amidinohydrolase)[12−16] is a binuclear manganese metalloenzyme responsible for the hydrolysis of L-arginine to L-ornithine and urea. The overall structure of the enzyme is shown in Figure 1. Each of the three identical subunits exhibits a characteristic α/β fold and possesses a pair of antiferromagnetically (AF) spin-coupled Mn(II) ions necessary for optimal activity. Two histidine (His101 and His126) and four aspartate residues (Asp124, Asp128, Asp232, and Asp234) as well as a bridging exogenous ligand (H_2O or OH^- ion) are directly coordinated to the Mn atoms. The proposed reaction mechanism[13,17,18] (see Figure 2) involves a nucleophilic attack of a bridging OH^- ion on the guanidinium group of arginine, resulting in the formation of a tetrahedral intermediate. The next step in the catalytic cycle is the collapse of the intermediate following proton transfer, likely through Asp128, to the leaving group (ornithine). The cycle is completed by the release of the products and the regeneration of the active

(1) Wilcox, D. E. *Chem. Rev.* **1996**, *96*, 2435−2458.
(2) Dismukes, G. C. *Chem. Rev.* **1996**, *96*, 2909−2926.
(3) Lipscomb, J. D.; Sträter, N. *Chem. Rev.* **1996**, *96*, 2375−2433.
(4) Pelletier, H.; Sawaya, M. R.; Kumar, A.; Wilson, K. S.; Kraut, J. *Science* **1994**, *264*, 1891−1903.
(5) Christianson, D. W. *Prog. Biophys. Mol. Biol.* **1997**, *67*, 217−252.
(6) Kimura, E. *Curr. Opin. Chem. Biol.* **2000**, *4*, 207−213.
(7) Barynin, V. V.; Whittaker, J. W.; Antonyuk, S. V.; Lamzin, V. S.; Harrison, P. M.; Artymiuk, P. J.; Whittaker, J. W. *Structure* **2001**, *9*, 725−738.
(8) Yoder, D. W.; Hwang, J.; Penner-Hahn, J. E. *Met. Ions Biol. Syst.* **2000**, *37*, 527−557.
(9) Jordan, A.; Reichard, P. *Annu. Rev. Biochem.* **1998**, *67*, 71−98.
(10) Wilce, M. C. J.; Bond, H. S.; Dixon, N. E.; Freeman, H. C.; Guss, J. M.; Lilley, P. E.; Wilce, J. A. *Proc. Natl. Acad. Sci. U.S.A.* **1998**, *95*, 3472−3477.
(11) Sträter, N.; Lipscomb, W. N. *Biochemistry* **1995**, *34*, 14792−14800.
(12) Lee, D.; Hung, P.-L.; Spingler, B.; Lippard, S. J. *Inorg. Chem.* **2002**, *41*, 521−531.
(13) Christianson, D. W.; Cox, J. D. *Annu. Rev. Biochem.* **1999**, *68*, 33−57.
(14) Ash, D. E.; Cox, J. D.; Christianson, D. W. *Met. Ions Biol. Syst.* **2000**, *37*, 407−428.
(15) He, C.; Lippard, S. J. *J. Am. Chem. Soc.* **1998**, *120*, 105−113.
(16) Cox, J. D.; Kim, N. N.; Traish, A. M.; Christianson, D. W. *Nat. Struct. Biol.* **1999**, *6*, 1043−1047.
(17) Kanyo, Z. F.; Scolnick, L. R.; Ash, D. E.; Christianson, D. W. *Nature* **1996**, *383*, 554−557.
(18) Khangulov, S. V.; Sossong, T. M.; Ash, D. E.; Dismukes, G. C. *Biochemistry* **1998**, *37*, 8539−8550.

10.1021/ja043693i CCC: $30.25

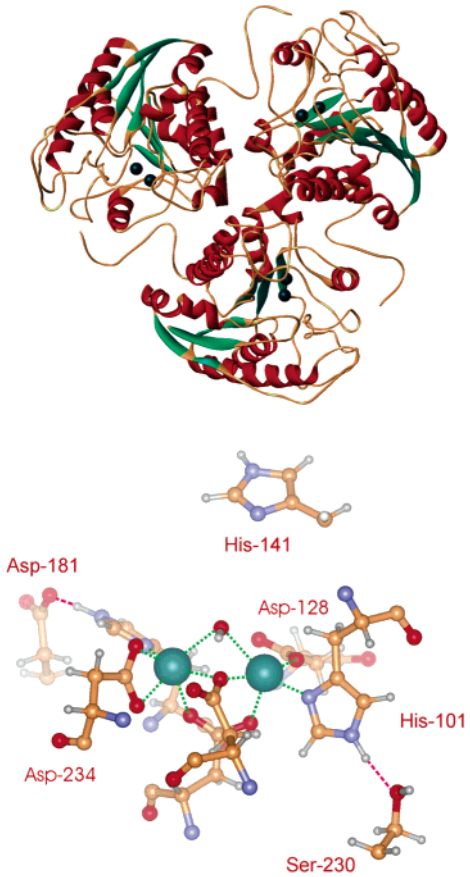

Figure 1. (Top panel) α/β fold characteristic of arginase. (Bottom panel) Arginase active site. Coordination and hydrogen bonding patterns are indicated by dotted lines in green and red, respectively.

nucleophile. Chelating agents can be used to extract the more weakly bound manganese atom (Mn_A) to produce a half active, metal-depleted state of the enzyme. Thus, arginase can function in principle as a mononuclear hydrolase, albeit with reduced activity.[13,19] In the present work, we have focused on the last step in the catalytic cycle, the regeneration of the nucleophilic hydroxide moiety. We attempt to address the following questions: do dynamical rearrangements occur in the dimetal cluster on a time scale that we can simulate, and if they do, are they relevant to catalysis? Can Asp128 serve as a proton shuttle as implied by the proposed mechanism? Does the exogenous water molecule occupy a bridging or terminal position, and how does this position affect its nucleophilic character?

The paper is organized as follows: (i) computational details are provided in section 2; (ii) in section 3.1 we trace the time evolution of key coordination bonds and comment on the observed repeated proton-transfer attempts to the Asp128 residue; (iii) in section 3.2 we quantify the proton-transfer processes and the concomitant changes in metal coordination by constructing two-dimensional histograms in terms of simple, yet representative, internal coordinates; (iv) section 3.3 contains the results from constrained dynamics simulations of the proton transfer, which complement the previous analysis and allow more rigorous comparison between the native and metal-depleted forms of the enzyme; (v) finally, in section 4 we present our conclusions and directions for future work.

(19) Scolnick, L. R.; Kanyo, Z. F.; Cavalli, R. C.; Ash, D. E.; Christianson, D. W. *Biochemistry* **1997**, *36*, 10558−10565.

2. Computational Details

An investigation of two models for the active site of rat liver arginase was carried out using finite temperature ab initio molecular dynamics (AIMD). All calculations utilized the Car Parrinello extended Lagrangian formulation of AIMD and were performed with the program CPMD.[20,21] The gradient corrected exchange-correlation functional of Becke and Perdew (BP)[22,23] was adopted for the present study. To account for the valence-core interactions we employed an analytical von Barth and Car pseudopotential for hydrogen and norm-conserving Troullier−Martins pseudopotentials[24] for all other elements. For manganese the nonlocal part of the pseudopotential was integrated numerically using a Gauss−Hermite quadrature, whereas for the rest of the atoms we used the Kleinman−Bylander[25] scheme. The valence electronic wave functions were expanded in a plane wave basis set with an energy cutoff of 100 Ry based on convergence results from small molecule calculations on Mn(II) compounds. All hydrogen nuclei were replaced by deuterium. A fictitious electronic mass of 900 au (1000 au for the constrained dynamics runs) was selected, which permitted the integration of the equations of motion with a time step of 0.125 fs (5.0 au). This set of parameters ensured adiabatic conditions for the electrons and good control over the conserved quantities. Starting with optimized structures from a previous study of rat liver arginase,[26] two models for the active site were constructed. They differed in the number of metal centers (native versus metal-depleted, Figure 3) and the protonation state of the backbone nitrogen atoms of Asp232 and Ser230 (adjusted to ensure overall neutrality). The peptide bond carbon and nitrogen atoms as well as the α carbon atom were restrained to their crystallographic positions, leaving the side chains to move freely. Valence saturation was modeled by capping with hydrogen atoms. The models, which contained around 100 atoms, were introduced into orthorhombic cells of appropriate dimensions (13.5 Å × 13.5 Å × 11.5 Å), chosen as a good compromise between computational efficiency and the need to sufficiently separate the periodic images. In both cases the active site was solvated with water to ensure a density of 1 g/cm^3 for the two systems. The choice to solvate was based on classical molecular dynamics runs for the entire enzyme, which revealed that the active site was readily accessible to the solvent when no substrate molecule was bound to it. Periodic boundary conditions were employed. To account for the presence of open shell orbitals on the Mn atoms we employed spin-unrestricted DFT methodology based on the local spin density approximation (LSD). For the metal-depleted form of arginase, a multiplicity of 6 was selected. For the native form of arginase, instead of performing the calculations for the antiferromagnetic (AF) state, which is the true ground state in the spin state manifold, we have restricted our models to reflect ferromagnetic coupling. Thus, we have fixed the multiplicity of the manganese atoms pair to the highest possible value. This approximation has been widely employed in DFT studies of transition metal systems and its success is based on the small energetic effect of the coupling[27] (it is generally, less than 1 kcal/mol and below the inherent accuracy of the DFT functional). The dynamics simulations on the two model systems were performed for ∼10 ps in the NVT ensemble. The temperature was maintained at ∼300 K by the use of Nose−Hoover thermostats with a chain length of four and target frequency of 500 cm^{-1}. For the constrained dynamics runs we enforced deprotonation,

(20) Car, R.; Parrinello, M. *Phys. Rev. Lett.* **1985**, *55*, 2471−2474.
(21) Hutter, J.; Alavi, A.; Deutsch, T.; Bernasconi, M.; Goedecker, St.; Marx, D.; Tuckerman, M.; Parrinello, M. *CPMD*, version 3.4; MPI für Festkörperforschung and IBM Research Laboratory: Stuttgart and Zurich, 1995−2000.
(22) Becke, A. D. *Phys. Rev. A: At., Mol., Opt. Phys.* **1988**, *38*, 3098−3100.
(23) Perdew, J. P. *Phys. Rev. B: Condens. Matter* **1986**, *33*, 8822−8824.
(24) Troullier, N.; Martins, J. L. *Phys. Rev. B: Condens. Matter* **1991**, *43*, 1993−2006.
(25) Kleinman, L.; Bylander, D. M. *Phys. Rev. Lett.* **1982**, *48*, 1425−1428.
(26) Ivanov, I.; Klein, M. L. *Proteins: Struct., Funct., Genet.* **2004**, *54*, 1−7.
(27) Siegbahn, P. E. M. *Theor. Chim. Acta* **2001**, *105*, 197−206.

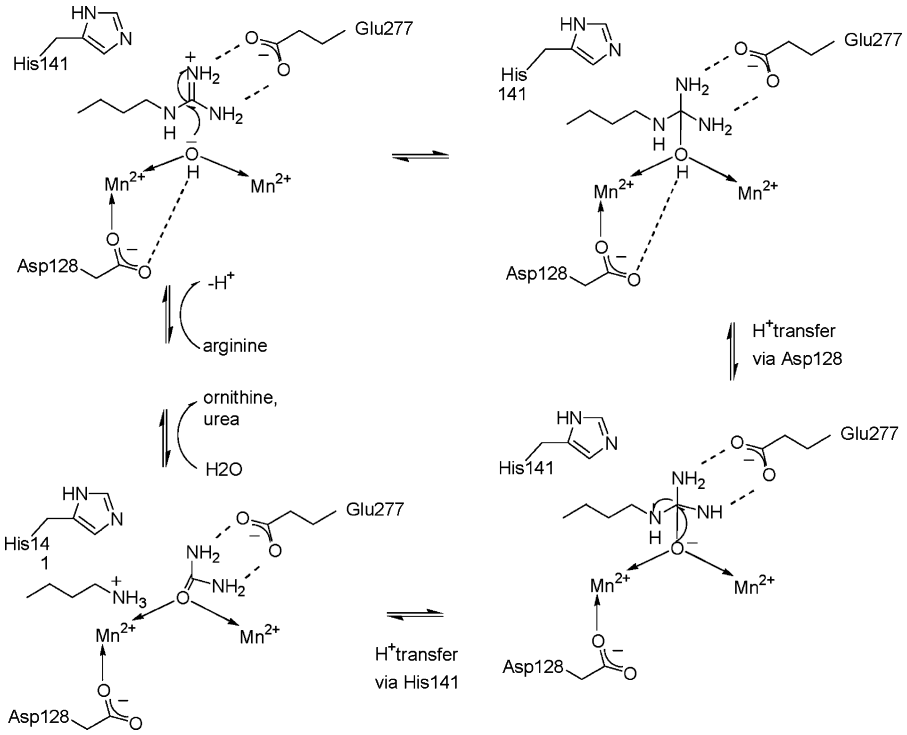

Figure 2. Mechanism for L-arginine hydrolysis proposed by Christianson et al. involving nucleophilic attack from the bridging position in the binuclear metal motif of arginase.

through the use of a control parameter δ (asymmetric stretch coordinate), defined as follows:

$$\delta = (d_{O^*-H} - d_{H-O'}) \quad (1)$$

where d_{O^*-H} and $d_{H-O'}$ are the distances indicated in Figure 4 and O* and O′ are the oxygen atom of the bridging water molecule and the oxygen atom of Asp128, which confine the mobile proton H. The values of δ were then varied in increments of 0.1 Å from −0.8 to 0.8 Å, and constrained trajectories of length ∼3 ps (∼1 ps of equilibration and 2 ps of production dynamics) were obtained for each discrete value of the control parameter.

3. Results and Discussion

3.1. Time Evolution of Characteristic Distances. As a first goal in our direct dynamics simulation of the arginase active site, we set out to characterize the motions of all first-shell ligands and establish the magnitude of deviation from the crystal structure of native arginase. To this end, we examined the time evolution of some critical coordination distances. Table 1 presents these results in compact form and contains the average Mn−O and Mn−N coordination distances from our simulation as well as the corresponding bond lengths from the crystal structure. The issue of reliability of the experimental structural parameters should be critically assessed, when making comparisons to ab initio calculations. The crystal structure of native arginase, on which our models are largely based, was determined at a 2.10 Å resolution.[13,17] A rough estimate of the uncertainty in the Mn−O* bonds can be obtained by looking at these distances in the three identical subunits. The average of all six distances is 2.402 Å with a standard deviation of 0.12 Å. This is consistent with an upper limit root-mean-square (rms) coordinate error of ∼0.2 Å obtained from a Luzzati plot (D. W. Christianson, personal communication) and is not atypical for structures obtained at that resolution. Overall the results indicate that the dimanganese structural motif possesses substantial flexibility as evidenced by the large rms values associated with the intermetal distance, the O−Mn coordination distances of the terminal Asp234 residue and the metal-bridging water molecule. The variation in O*−$Mn_{A,B}$ distances highlighted the considerable mobility of the bridging nucleophilic water molecule, which was found to move from bridging to terminal positions involving both Mn_A and Mn_B. These findings are also reflected in the computed B-factors from our dynamics runs (presented in Figure 6b), which give an idea about the magnitude of deviation in the positions of the coordinating atoms due to thermal motion. Again the coordinating O atoms of Asp234 and the dangling O atom of the μ-1,1 bridging Asp232 displayed the largest range of motion. Individual snapshots taken from the trajectories differed from the optimized initial configuration, based on the crystal structure. However, when averaged over the length of the trajectory the atomic positions were in remarkably close agreement with the crystallographic values. This reflects the overall stability of the dimetal structural motif (maintained primarily through coordination to the metals) and the fact that it represents a minimum on the free energy surface independent of tethering to the protein scaffold or the presence of second-shell ligands. Visual inspection of the trajectory for the native arginase model revealed an intriguing repeated proton transfer from the bridging water molecule to the dangling oxygen of the Asp128 residue. No proton transfer was observed in the case of metal-depleted arginase, although a short strong hydrogen bond was maintained between the two ligands throughout our simulations. Asp128 has been implicated as catalytically essential by mutagenesis studies,[29] which

(28) Mei, H. S.; Sagnella, D. E.; Klein, M. L.; Tuckerman, M. E. *J. Phys. Chem.* **1998**, *102*, 10446−10458.
(29) Cama, E.; Emig, F. A.; Ash, D. E.; Christianson, D. W. *Biochemistry* **2003**, *42*, 7748−7758.

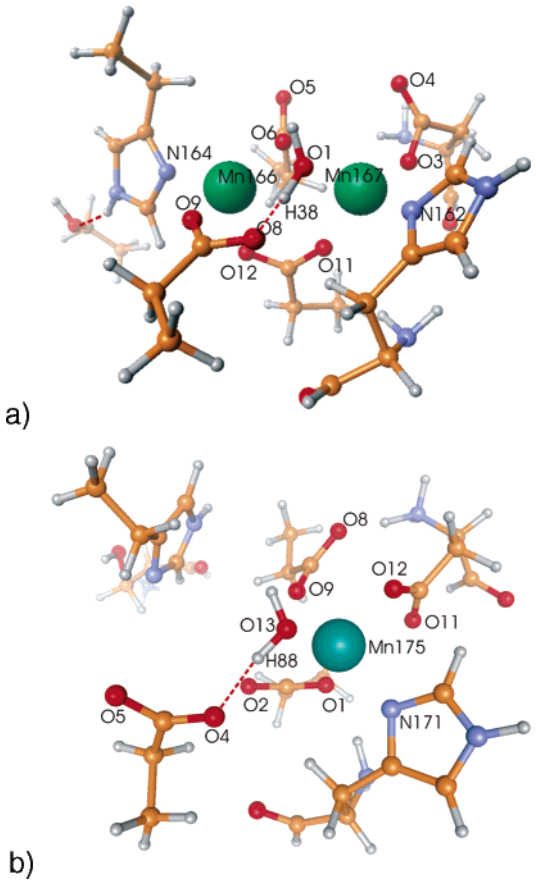

Figure 3. Models for the active site of native (a) and metal-depleted (b) arginase. Atoms are color coded as follows: carbon in gold; hydrogen in gray; nitrogen in blue; oxygen in red; and manganese in green. Hydrogen bonding patterns are indicated by dotted lines in red. The labels denote the type and numbering of the atoms coordinated to the dimetal manganese core of the active site. The atom-numbering scheme is the same as the one used in Figure 6.

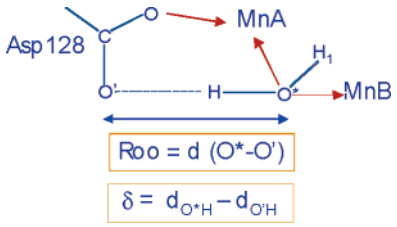

Figure 4. Schematic representation of the internal coordinates relevant to proton transfer between the nucleophilic water molecule and Asp128.

demonstrated that mutations in this residue abolish the activity of the enzyme. It also plays a prominent role in the proposed catalytic mechanism, serving as a proton shuttle during the collapse of the tetrahedral intermediate, following the initial nucleophilic attack. Shown in Figure 5a is the time evolution of distances relevant to the process of proton transfer (see also Figure 4). The hydrogen atom of the bridging water molecule makes brief excursions to reside at the dangling oxygen atom of Asp128 (O′). The proton transfer occurs very infrequently and is accompanied by a number of recrossing events. This can be explained by the asymmetry of the free energy well for H* and the finite free energy difference, separating states in which the mobile proton resides on the water oxygen O* from the states in which it is located on the aspartate oxygen O′. Therefore, we conclude that proton transfer in this case is a

Table 1. Table of Characteristic Distances[a]

distance (Å)	X-ray	native	metal-depleted	σ(native)	σ(metal-depleted)
$Mn_A-N\delta$(His101)	2.24	2.14		0.16	
$Mn_B-N\delta$(His126)	2.09	2.15	2.28	0.15	0.11
Mn_A-O1(Asp124)	2.03	2.09		0.21	
Mn_B-O2(Asp124)	2.05	2.08	2.03	0.21	0.07
$Mn_A-O^*(H_2O/OH^-)$		2.59		0.46	
$Mn_B-O^*(H_2O/OH^-)$		2.42	2.25	0.35	0.17
O*−O1(Asp128)		2.64	2.75	0.40	0.17
O2(Asp128)$-Mn_A$	2.75	2.02		0.27	
Mn_A-O1(Asp232)	2.46	2.11		0.17	
Mn_B-O1(Asp232)	2.29	2.36	2.21	0.49	0.14
Mn_B-O1(Asp234)	2.11	2.07	2.25	0.17	0.26
Mn_B-O2(Asp234)	2.39	3.16	2.62	1.00	0.35
Mn_A-Mn_B	3.32	3.39		0.79	

[a] Presented are the distances from the crystal structure; averaged distances for native and metal-depleted arginase from the direct dynamics runs and the corresponding standard deviations σ (in Å)

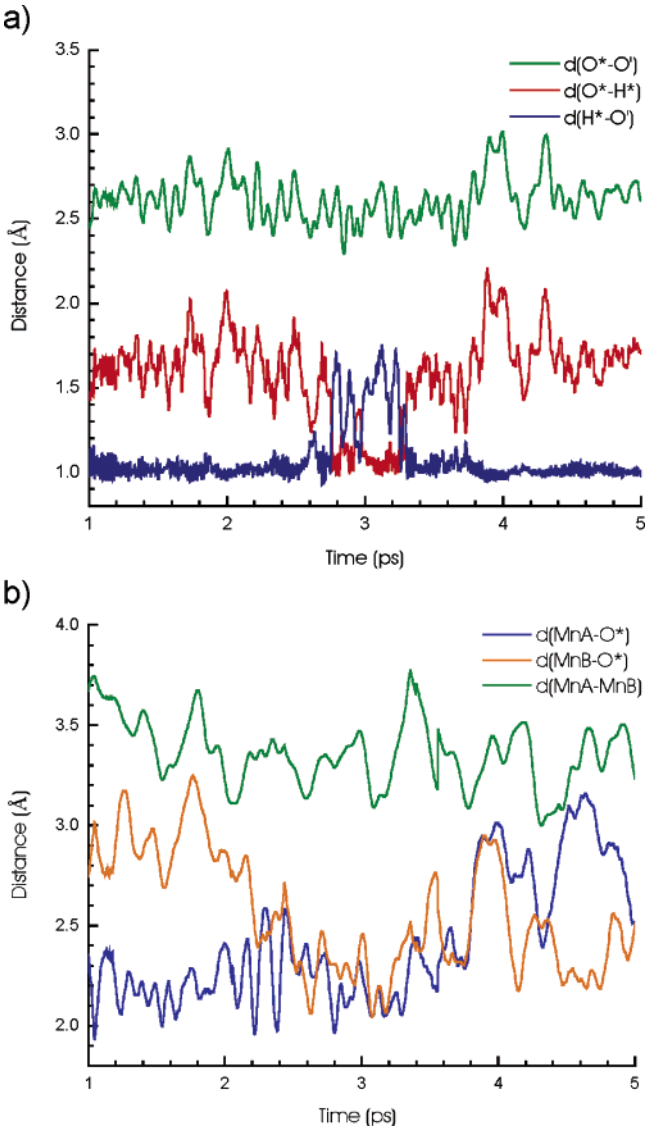

Figure 5. (a) Time evolution of distances characteristic of the proton-transfer events to Asp128; d_{O^*-H}, $d_{H-O'}$, and $d_{O^*-O'}$ are represented in red, blue, and green, respectively. (b) Time evolution of manganese−manganese and manganese−oxygen coordination distances indicated by lines in green, blue, and orange.

rare event on the CPMD time scale, unlike proton transfer of a hydronium ion in aqueous solution (via the Grotthus mecha-

nism), which occurs on a time scale of a few hundred femtoseconds and with no barrier.[28] In Figure 5b we have plotted the Mn_A-Mn_B distance and the Mn_A-O^*, Mn_B-O^* coordination distances as a function of time over the same time period as in Figure 5a, in order to allow for comparison. Our computed distances vary along the trajectory from ~3.0 Å to ~3.7 Å, with an average centered at about 3.3 Å. The potential energy surface is rather flat in the direction of the Mn_A-Mn_B mode, which explains the relatively wide range of intermetal distances observed experimentally (~3.3 Å from the crystal structure[17] and ~3.36−3.57 Å from the analysis of zero field splittings in the EPR spectra[14,30]). There is no significant correlation between that mode and the proton transfer occurring in the system for the native arginase active site. The Mn_A-O^* and Mn_B-O^* distances also vary in a wide range, reflecting the flexible coordination of the bridging nucleophilic water molecule and the fact that it continually switches between terminal and bridging position with respect to the two metal sites. In fact, within the limited stretch of trajectory shown, we find it coordinated to Mn_A first, then coordinated to both metal atoms and finally coordinated to Mn_B only. It is interesting to note that when the proton transfer occurs the water molecule is either bound to Mn_A or bridging and departure to the Mn_B atom terminates the proton-transfer attempts.

We have also examined the covariance and cross correlation (normalized covariance) matrices for the atoms in our system. If the positions of two atoms i and j at time t are $r_i(t)$ and $r_j(t)$ the corresponding covariance matrix element can be obtained from the following expression:[31,32]

$$c_{ij} = \langle (r_i - \langle r_i \rangle) \cdot (r_j - \langle r_j \rangle) \rangle = \langle r_i . r_j \rangle - \langle r_i \rangle \langle r_i \rangle$$
$$= \frac{\Delta t}{t_{av}} \left(\sum_{t=0}^{t_{av}-\Delta t} r_i(t)\, r_j(t) - \frac{\Delta t}{t_{av}} \left(\sum_{t=0}^{t_{av}-\Delta t} r_i(t) \right) \times \left(\sum_{t=0}^{t_{av}-\Delta t} r_j(t) \right) \right) \quad (2)$$

where t_{av} is the averaging time, Δt is the time step, and the angular brackets denote time averaging. The diagonal elements of the covariance matrix represent the mean square fluctuations of the atoms and are related to the computed B-factors by a constant multiplicative factor $8\pi^2/3$. The cross correlation matrix elements are defined as[31]

$$c_{ij} = \frac{c_{ij}}{c_{ii}^{1/2}\, c_{jj}^{1/2}}$$

and range from −1 to 1. Unlike the covariance coefficients, they do not contain any information about the magnitude of the correlated motions. In Figure 6a and b we have plotted the calculated covariance and cross correlation coefficients between the mobile H atom and all atoms coordinated to the dinuclear manganese core. In Figure 6c we have shown the computed B-factors for all atoms involved in metal coordination. Experience from classical molecular dynamics simulation[31] has shown that caution should be exercised when comparing these values to the experimental B-factors, and we have not attempted to do so. The fact is that the elements of the covariance matrix in proteins may not converge for a number of nanoseconds, and

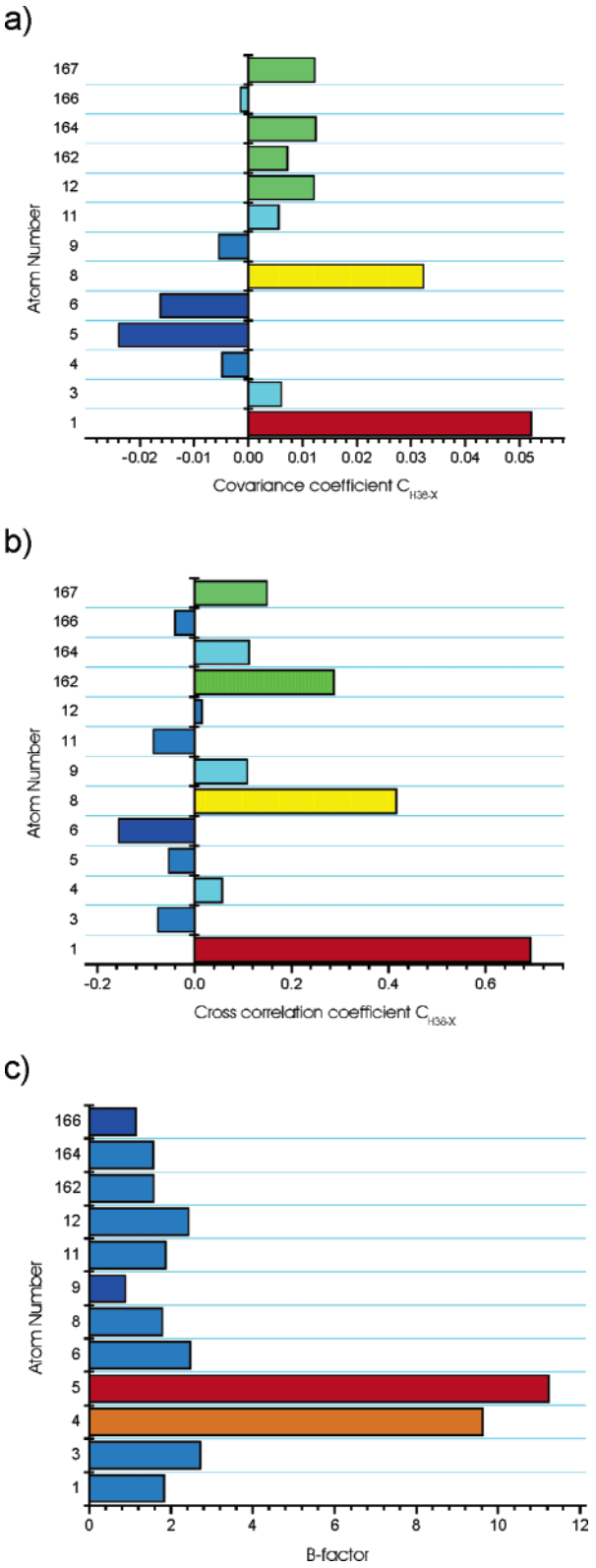

Figure 6. (a) Covariance coefficients between the mobile H atom and various metal-coordinating atoms in the active site of native arginase; (b) Analogous cross correlation coefficients. (c) Computed B-factors for various metal-coordinating atoms in the active site of native arginase. The color scheme indicates the magnitude of the coefficients and spans a range of colors from blue (smaller values) to red (larger values). The atom-numbering scheme is the same as the one used in Figure 3.

(30) Khangulov, S. V.; Pessiki, P. J.; Barynin, V. V.; Ash, D. E.; Dismukes, G. C. *Biochemistry* **1995**, *34*, 2015−2025.
(31) Hunenberger, P. H.; Mark, A. E.; van Gunsteren, W. F. *J. Mol. Biol.* **1995**, *252*, 492−503.
(32) Ichiye, T.; Karplus, M. *Proteins: Struct., Funct., Genet.* **1991**, *11*, 205−217

even in that case it is not straightforward to carry out a meaningful comparison as the experiment is done under different conditions and on a vastly different time scale. Fortunately, in this article we are not concerned at all with large-scale protein motions, which are the domain of classical molecular dynamics. We would rather examine the short time scale motions of the first-shell ligands, commensurate with the time scale of the observed proton transfer in the active site. It is evident from Figure 6a that the atoms displaying the largest covariance with the motion of the mobile proton are the flanking oxygen atoms O* (1) and O′ of Asp128 (8). What is, perhaps, surprising is the strongly anti-correlated motion of the two oxygen atoms of the $\mu-1,1$ bridging Asp232 residue. We attribute this fact to the departure of Asp232, which binds more strongly to Mn_A whenever the bridging water molecule (and with it the proton H) moves to associate more closely with Asp128. Anticipating our results, (see details in section 3.3) we mention that the strong cross correlation in this case is consistent with the observation from our constrained molecular dynamics runs that the Asp232 residue serves as a departing ligand during proton transfer. We also note that there is very little correlation between the motion of the mobile hydrogen atom and the motion of the terminal Asp234 residue, even though Figure 6c suggests that it undergoes the largest motions as evidenced by the B-factors of its two oxygen atoms. This can mean either that the motions are completely uncorrelated or, alternatively, that they occur in perpendicular directions, in which case the cross correlation coefficients c_{ij} vanish. The source of the large B-factors becomes readily apparent upon visual inspection of the trajectories: Asp234 switches continuously between syn-monodentate and syn-bidentate coordination. Such carboxylate shifts[33−35] are generally considered important for catalysis and have been suggested as a potential way for an enzymatic active site to accommodate substrate binding during catalytic turnover. The fact that the Asp232 and Asp234 residues display the largest degree of structural variability is not altogether unexpected. In a previous study[26] involving static DFT calculations on arginase models, analysis of the electronic properties of the active site revealed that orbitals involving the terminal Asp234 residue as well as the flexible μ-1,1 bridging Asp232 lie at high energies, close to the HOMO−LUMO gap. This observation is consistent with weak coordination of these residues and suggests them as departing ligands should any rearrangements occur in the active site. Very recent crystallographic data on human arginase II has shown structural variability in the position of the residue analogous to Asp232, which is consistent with our findings.[34,35]

3.2. Effective Free Energy and Potential of Mean Force Profiles. To examine the proton transfer in the active site of arginase in more detail, we have constructed two-dimensional histograms, reflecting the joint probability $P(R_{O-O}, \delta)$ to observe a particular value of the asymmetric stretch coordinate δ and a particular value of the distance X−X′, where X−X′ represents the following pairs of atoms: (i) O*−O′; (ii) Mn_A-Mn_B; (iii) Mn_A−O*; (iv) Mn_B−O*; and (v) $Mn_{A,B}$−O1(Asp232). The asymmetric stretch coordinate is useful in the analysis of individual localized proton motions between the two oxygen atoms O* and O′ and in determining the extent of correlation between the motion of the mobile proton H and the motions of other atoms coordinated to the dimetal core of the active site.

From the two-dimensional histograms it is straightforward to obtain effective free energy surfaces[28] using the following expression from statistical mechanics:

$$F = -\beta^{-1} \ln P(R_{X-X'},\delta) \tag{4}$$

where $P(R_{X-X'},\delta)$ is the above-mentioned two-dimensional distribution function and β is the inverse of k_BT (the Boltzmann constant multiplied by the absolute temperature T in K). In Figure 7 we have contrasted the case of native versus metal-depleted arginase by projecting the effective free energy surface on two simple, yet representative, internal coordinates, δ and $R_{O^*-O'}$. For ease of comparison, on the left side we have presented a 3D surface and a corresponding 2D contour plot for the case of native arginase, whereas on the right we have plotted similar free energy surfaces for the metal-depleted form of the enzyme. When both manganese centers are present, we observe an elongated, strongly asymmetric, double well potential, extending from $\delta \approx -1.2$ Å to 0.8 Å. The center of the deepest free energy minimum, found on the left-hand side of the contour graph, corresponds to an $R_{O^*-O'}$ distance of ∼2.65 Å and a value of $\delta \approx -0.65$ Å. It represents the case when the mobile H atom is stably bound to the oxygen atom O*, forming the bridging nucleophilic water molecule. The shallow energy minimum on the right-hand side of the graph (centered at $R_{O^*-O'} \approx 2.6$ Å and a value of $\delta \approx 0.45$ Å) represents the case when the mobile proton has migrated to the O′ atom of Asp 128, leading to the formation of a hydroxide moiety in the bridging position. It is evident that a water molecule bridging the two metals is considerably more stable than the deprotonated form, with the proton residing on Asp128. It is also readily apparent that the barrier for reverse proton transfer, separating states with negative from states with positive values of δ, is very small, on the order of the energy of the thermal fluctuations. It is likely that inclusion of nuclear quantum effects, which were not accounted for in our simulations, would have resulted in the complete disappearance of the barrier and the formation of a single-well hydrogen bond potential between the two oxygen atoms. In view of the above, it is understandable why the proton makes only brief excursions in the direction of the O′ atom and comes back to reside on the bridging water molecule on a time scale commensurate with just a few vibrational motions of the oxygen atoms. We also observe that the $R_{O^*-O'}$ mode is strongly correlated with the motion of the hydrogen atom, as expected in proton transfer. The value of the $R_{O^*-O'}$ distance decreases to ∼2.4 Å in the region connecting the two potential wells at values of $\delta \approx 0$ Å. This reflects the well-established fact that the proton migration events occur with high probability only when the distance separating the heavy atoms is sufficiently small.

In the case of metal-depleted arginase, the effective free energy surface is dramatically different. We observe only one local minimum centered at $R_{O^*-O'} \approx 3.0$ Å and a value of $\delta \approx -0.8$ Å. Similar to the case of native arginase, the $R_{O^*-O'}$ distance is correlated with the motion of the hydrogen atom, although less strongly, as evidenced by the less elongated shape of the free energy minimum. This is consistent with the observation of a persistent hydrogen bond between the metal-

(33) Torrent, M.; Musaev, D. G.; Morokuma, K. *J. Phys. Chem. B* **2001**, *105*, 322−327.
(34) Magistrato, A.; DeGrado, W. F.; Laio, A.; Rothlisberger, U.; VandeVondele, J.; Klein, M. L. *J. Phys. Chem. B* **2003**, *107*, 4182−4188.
(35) Papoian, G. A.; Klein, M. L.; DeGrado, W. F. *J. Am. Chem. Soc.* **2003**, *125*, 560−569.

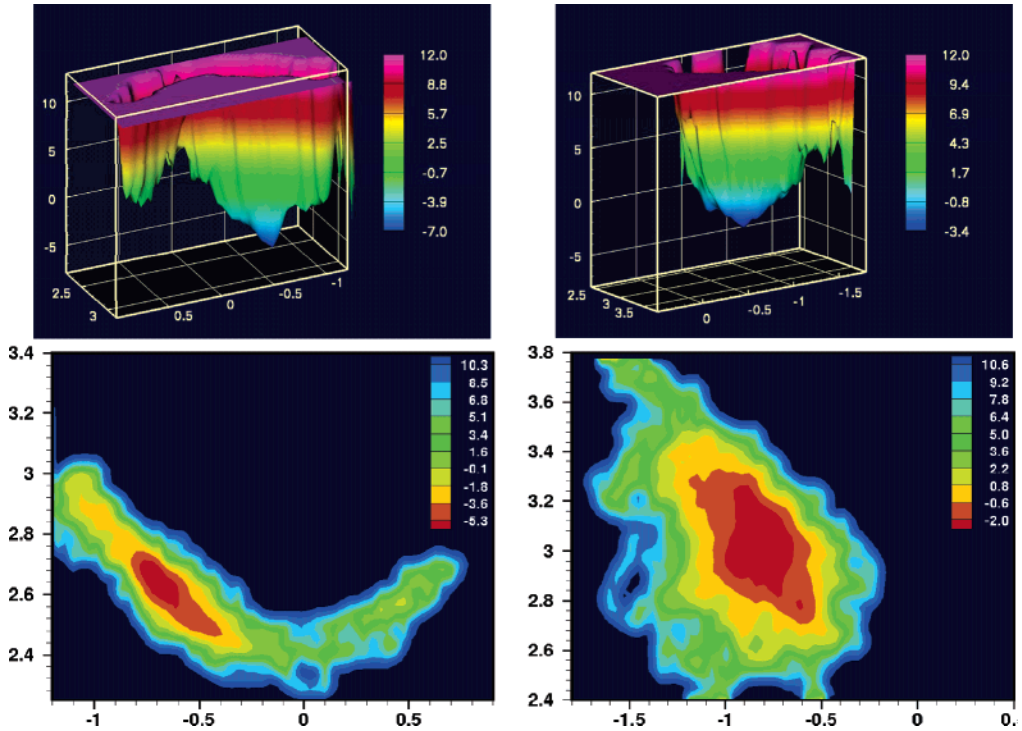

Figure 7. Two-dimensional effective free energy surfaces, depicting F as a function of the asymmetric stretch coordinate δ and R_{O-O} distance at 300 K. The 3D surface (top) and corresponding 2D contour plots are shown on the left for native arginase. To the right are presented similar plots for the case of metal-depleted arginase. The units are in kcal/mol, and the reference level is chosen arbitrarily.

bridging water molecule and the Asp128 residue, which is marginally weaker than the one found in the native form of the enzyme. The fact that only negative values of δ are observed reflects the absence of proton transfer in the metal-depleted form of the enzyme. This is easily explained if we consider the pK_a lowering effect that metal coordination has on the nuclephilic water molecule. Coordination of a water molecule to a metal ion decreases the pK_a due to the electrostatic stabilization of the negatively charged hydroxide species. For instance, the pK_a of a water molecule in bulk solvent is 15.7, whereas the pK_a of metal bound water in the hexa-aquo complex of Mn^{2+} is ~10.5. Thus, a mononuclear manganese site is not expected to lower the pK_a of a bound water molecule sufficiently to match that of an Asp or Glu residue. This is precisely what we observe: due to the large free energy difference between the protonated and the deprotonated forms, no deprotonation is observed in the mononuclear site. Binding to two manganese centers draws a significant amount of charge and polarizes the bound water molecule to a much greater extent than binding to one manganese ion would. This, in turn, brings the pK_a of a bridging water molecule in a range much closer to 7, only a few kilocalories lower, in terms of free energy, than an aspartate residue. Thus, it is perfectly possible to observe, as we do, equilibrium between the two forms, although shifted heavily toward the more stable water molecule. While the presence of two positively charged cations in the motif aids in deprotonation of the bridging water molecule, the two metals have a very high affinity for the resulting negatively charged hydroxide species, leading to a decrease in its nucleophilic character. Optimal enzymatic function requires a precise balance between acidity and nucleophilicity, which has to be maintained through charge transfer from the first shell ligands, especially the negatively charged aspartate residues. Introducing electron-donating ligands into the first or second coordination spheres of the metals is expected to raise the pK_a of a metal coordinated solvent molecule. Conversely, the pK_a would be lowered by the lack of such ligands. The ionization of a metal-bridging water molecule results in the apparent pK_a of 7.9 observed experimentally in the pH−rate profile for arginase, with an optimum pH range for catalysis between 9 and 9.5.[37] The limited statistics that can be collected during direct AIMD simulation and the fact that the proton transfer occurs infrequently on the time scale that we can access preclude a more quantitative analysis of the multidimensional effective free energy surfaces. We have, therefore, limited the discussion to the more qualitative features of the potentials of mean force, which can be properly converged. We will revisit the topic of free energies in the next section, in which we discuss the results of constrained dynamics calculations intended to circumvent the problem of limited statistics in the observation of rare events.

We have also examined how the motion along the proton-transfer coordinate is correlated to the motion of the Mn atoms as well as the motion of the bridging monodentate Asp232 residue. Shown in Figure 8a−c are two-dimensional effective free energy surfaces depicting the free energy in terms of the asymmetric stretch coordinate and the intermetal distance Mn_A−Mn_B or the coordination distances Mn_A−O* and Mn_B−O*, respectively. What we can immediately conclude from examining the graphs is that the Mn_A−Mn_B distance is not strongly correlated to the proton-transfer coordinate. Two minima are observed in Figure 8a: one (on the left), corresponding to the bridging water molecule and, the other (on the right), to the

(36) Cama, E.; Colleluori, D. M.; Emig, F. A.; Shin, H.; Kim, S. W.; Kim, N. N.; Traish, A. M.; Ash, D. E.; Christianson, D. W. *Biochemistry* **2003**, *42*, 8445−8451.
(37) Kuhn, N. J.; Talbot, J.; Ward, S. *Arch. Biochem. Biophys.* **1991**, *286*, 217−221.

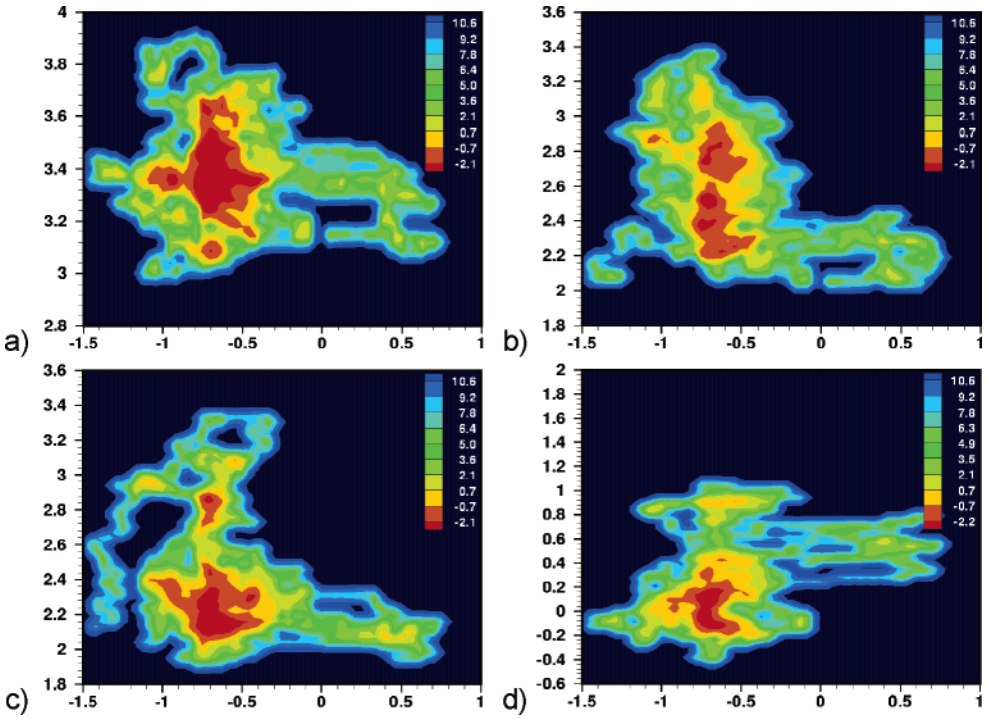

Figure 8. Two-dimensional effective free energy surfaces, depicting F as a function of the asymmetric stretch coordinate δ and $R_{X-X'}$ distance at 300 K, where X−X′ represents the following pairs of atoms: (a) Mn_A-Mn_B; (b) Mn_A-O^*; (c) Mn_B-O^*; and (d) $Mn_{A,B}-O1(Asp232)$.

hydroxide moiety. The larger minimum on the left extends from ∼3.0 Å to ∼3.7 Å for the values of $R(Mn_A-Mn_B)$ and from 0 Å to −1.4 Å for the values of δ. This reflects the very broad range of observed intermetal distances and once again identifies the manganese−manganese distance as a soft mode on the potential energy surface. The distances corresponding to positive values of δ tend to cluster in the lower range of intermetal distances, roughly between 3 and 3.4 Å, which is indicative of the fact that the bridging hydroxide, when it gets formed, is more strongly coordinated to the metal ions than the original water molecule and tends to bring them together.

Similar trends are exhibited by the graphs in Figure 8b and c, highlighting smaller coordination distances for the bridging hydroxide species. This trend is especially well pronounced in the graph depicting the Mn_A coordination, where we see the formation of a well-defined minimum at $d(Mn_A-O^*) \approx 2.1$ Å and $\delta \approx 0.5$ Å. The last of the four contour plots (Figure 8d) depicts the free energy surface in terms of δ and a parameter $\zeta = d(Mn_B - O1[Asp232]) - d(Mn_A - O1[Asp232])$. Here, ζ represents the difference in the coordination distances between the bridging oxygen of the monodentate Asp232 residue and Mn_A or Mn_B , respectively. We clearly see that the preferred position for Asp232 is bridging, exemplified by the broad minimum centered at $\zeta \approx 0$ Å and $\delta \approx -0.6/-0.7$ Å. However, we also observe a second shallow minimum at $\zeta \approx 0.8$ Å and $\delta \approx -0.4/-0.8$ Å signifying that Asp232 can also be asymmetrically bridging and associate more closely with Mn_A.

3.3. Constrained ab Initio Molecular Dynamics. In addition to direct AIMD dynamics, we have obtained accurate one-dimensional potentials of mean force (PMFs), corresponding to the deprotonation process in both the native and metal-depleted systems using constrained molecular dynamics. Constrained dynamics circumvents the statistical difficulties associated with the observation of rare events in straightforward molecular dynamics. In our case, we have utilized it to enforce deprotonation of the metal-bridging water molecule, using the asymmetric stretch coordinate as a preselected intuitive reaction coordinate. Thus, we have chosen $\delta = (d_{O^*-H} - d_{H-O'})$ as a control parameter for our constrained molecular dynamics runs and varied its value in the range from −0.8 Å to 0.8 Å with increments of 0.1 Å. For each constrained configuration we have obtained trajectories starting from well-equilibrated unconstrained configurations, taken from our direct AIMD simulations. After re-equilibrating for ∼1.0 ps the properties of interest were averaged for two additional picoseconds. The constraints were linearly added to the Car Parrinello Lagrangian according to the blue moon ensemble method.[38,39] The method corrects for the bias in the statistics for momentum space due to the introduction of constraints in coordinate space and has achieved wide popularity in the field of ab initio molecular dynamics.

Within this method the relative free energy between states ξ_0 and ξ_1 can be evaluated using the expressions[38]

$$\Delta F = -\int_{\xi_0}^{\xi_1} f_{\xi'}\, d\xi' \qquad f_{\xi'} = \frac{\langle Z^{-1/2}[\lambda - k_B TG]\rangle_{\xi'}}{\langle Z^{-1/2}\rangle_{\xi'}} \qquad (5)$$

where f_ξ is the average force of constraint; k_B is the Boltzmann constant; T is the temperature in K; Z and G are weight and correction factors, associated with the transformation from generalized to Cartesian coordinates. Since we have adopted a difference of distances as a control parameter in our simulations, the second equation reduces to a particularly simple form; it is just the ensemble average of the Lagrange multiplier λ.

The resulting potentials of mean force for native and metal-depleted arginase are presented in Figure 9. Each point in the

(38) Sprik, M.; Ciccotti, G. *J. Chem. Phys.* **1998**, *109*, 7737−7744.
(39) Carter, E. A.; Ciccotti, G.; Hynes, J. T.; Kapral, R. *Chem. Phys. Lett.* **1989**, *156*, 472−477.

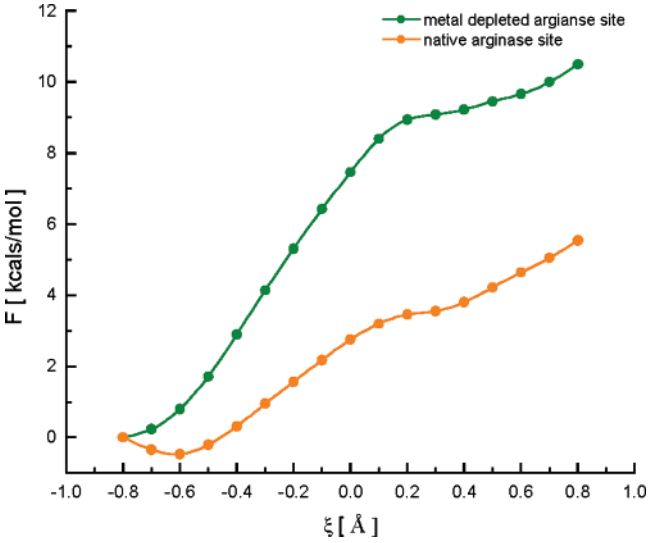

Figure 9. Potentials of mean force for the deprotonation in (i) native arginase (orange line) versus (ii) metal-depleted arginase (green line).

graph corresponds to a 3 ps constrained dynamics simulation. The two curves were obtained from thermodynamic integration of the constrained force f_ξ. Consistent with our observations from the previous section, we find that in the case of native arginase the minimum in the PMF is observed at $\xi \approx -0.6$ Å, whereas for the metal-depleted variant of the active site it is closer to -0.8 Å. On the left-hand side of the graph are states representing a stable metal bridging water molecule ($\xi < 0$ Å), and on the right-hand side are states in which the mobile proton H has been constrained to reside on the O′ atom of Asp128. The shape of the PMFs is precisely what we would expect, given our previous direct AIMD results: as the value of the constraint increases from left to right, we observe a steep initial increase in the free energy. Then the PMF levels off after the point $\xi \approx 0$ Å, which corresponds to the proton being equally shared by the two oxygen atoms O* and O′. After that point the free energy plateaus in the region up to $\xi \approx 0.4/0.5$ Å, corresponding to the stabilization of the deprotonated bridging hydroxide species. Further increases in the value of ξ result in increasing free energy. We should note that we do not observe a stable minimum in the PMF for the deprotonated form. The reason for this is two-fold. First, the minimum, as seen in the two-dimensional effective free energy surface, is very shallow, with an almost nonexistent barrier for the reverse recombination reaction. The second reason is associated with a deficiency of the difference constraint ξ. As the value of the control parameter gets increased, so does the total distance between the two oxygen atoms. For the extreme right side of the PMF this has the effect of pushing the metal-bridging hydroxide moiety and the aspartate residue apart. Any attempt to dislodge the hydroxide species from its stable bridging position is energetically unfavorable and is, therefore, accompanied by a free energy increase, as seen in the PMF.

The energetic implications of our calculated one-dimensional potentials of mean force are the following: (i) there is a substantial difference in the free energies of deprotonation through the Asp128 residue between the native and metal-depleted models of the active site; (ii) in the metal-depleted form this free energy difference is sufficiently large (~9 kcal/mol) to prevent the observation of proton transfer to Asp128. In our simulations Asp128 was modeled as acetate. Assuming an unaltered pK_a for acetate as a reference (pK_a~4.7), it is easy to estimate that a free energy difference of 4.27 kcal/mol (obtained by integrating the native arginase PMF from its mimum at $\delta \approx -0.6$ Å to $\delta \approx 0.4$ Å at the end of the plateau) would result in an estimated pK_a of 7.7 for the bridging nucleophile. Correspondingly, for the metal-depleted case a free energy difference of 9.22 kcal/mol (integration from $\delta \approx -0.8$ Å to $\delta \approx 0.4$ Å) would lead to an estimated pK_a value of 11.4. While these values should be regarded as highly approximate, given the significant simplifications and assumptions inherent to our models, they fall in the experimentally expected range and reflect the fact that two manganese ions depress the pK_a of a metal bridging water molecule much more effectively than a single Mn atom would, thus, promoting the formation of the putative nucleophilic hydroxide species. This fact has mechanistic relevance for arginase, as it may explain why a metal-deficient active site retains partial activity. The activity of the metal-loaded versus the metal-depleted form of the enzyme would be determined by the ratio of the concentrations of the nuclephilic hydroxide species, which is determined by the ability of each form to polarize an exogenous water molecule. More broadly, these results provide an indication as to why dinuclear metals sites may be favored in enzymatic hydrolysis.

We have also examined some ensemble averaged structural properties for different values of the distance constraint ξ in order to follow structural changes accompanying the deprotonation process. Results are presented in Figure 10a−c. First, we comment on the evolution of the coordinates directly involved in proton transfer as a function of the control parameter. We note the gradual increase in the average O*−H bond length and the simultaneous decrease in the H−O′ bond distance as the ratio between the two is being varied. In agreement with our previous observations, the average $R_{O^*-O'}$ distance goes though a minimum corresponding to $\xi = 0$ (H being equidistant from the two oxygen atoms). In Figure 10b we present the average intermetal and $Mn_{A,B}$−O* coordination distances as a function of ξ. The average Mn−Mn distance varies from ~3.2 Å to ~3.4 Å with rather substantial fluctuation from point to point in the curve. This is an indication that the intermetal distance takes on a relatively wide range of values and, therefore, cannot be properly averaged within the 2 ps duration of a constrained trajectory. Likewise, the large variation in the Mn−O* coordination distances is indicative of the labile binding of the bridging water molecule to Mn_A and Mn_B, respectively. The third panel of Figure 10 depicts the average coordination distances between the aspartate (Asp124, Asp232, Asp234) oxygen atoms and the manganese atoms. It is evident that most coordination distances are clustered around 2.1 Å with two notable exceptions: (i) the more distant oxygen of Asp234 shows considerable structural variability, due to its labile binding to Mn_B; (ii) the bridging oxygen atom of the monodentate μ-1,1 bridging Asp232 residue displays pronounced flexibility. More importantly, we observe that for negative values of the control parameter ξ the values for the coordination distance are similar to those of other coordinating aspartates, such as Asp124. By contrast, for positive values of ξ we detect significant departure of the Asp232 residue away from Mn_B, exemplified by an increase in the coordination distance from ~2.2 Å to ~2.6/2.8 Å. This is in accord with our previous observation, which

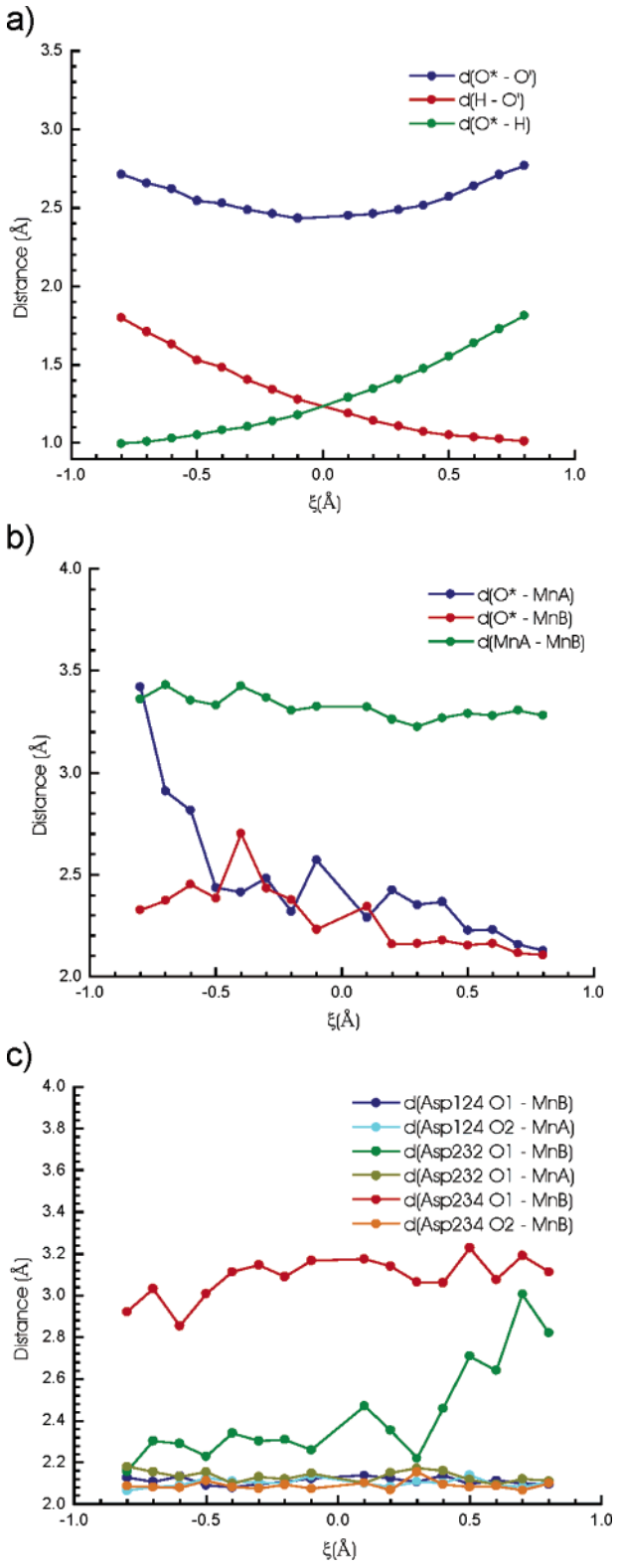

Figure 10. Average structural parameters as a function of the constrol parameter ξ. Shown are (a) coordinates directly involved in proton transfer; (b) average intermetal and $Mn_{A,B}$−O* coordination distances; (c) average aspartate coordination distances.

suggested Asp232 as a potential departing ligand. It has been proposed in the literature that the strong hydrogen bonding between the bridging water molecule and the terminal Asp128 residue may serve a dual purpose. First, it may facilitate the formation of the active nucleophile OH^- through proton transfer along the O−H···O coordinate. Second, the decreased ability of the resulting protonated aspartate to stabilize the positive charge on Mn_A may result in increased Lewis acidity at the metal cluster. In light of this, the observed departure of Asp232 from Mn_B to associate more closely with Mn_A can be viewed as a compensatory motion, which would counter the enhancement in the positive charge on the manganese atom through increased charge transfer from the aspartate residue.

3.4. Electron Localization Function. Finally, we have analyzed the deprotonation occurring in the native arginase active site in terms of changes in electronic structure. Namely, we have taken snapshots from our direct dynamics trajectory during one of the observed proton migration events and calculated the electron localization function (ELF). The electron localization function, proposed by Becke and Edgecombe,[40−43] can serve as a convenient tool for monitoring bond-breaking processes. For a closed-shell system, the ELF is defined as the inverse of a parameter χ, which represents the difference between the electronic kinetic energy density for the system under consideration with and without Pauli exclusion, normalized by the Thomas−Fermi energy term (the electronic kinetic energy density of the uniform electron gas). For a spin-unrestricted calculation, this definition can be generalized as follows:[40]

$$\mathrm{ELF} = \frac{1}{(1+\chi)^2} = \left[1 + \left(\frac{t_{P,\alpha} + t_{P,\beta}}{t_{h,\alpha} + t_{h,\beta}}\right)^2\right]^{-1} \tag{6}$$

$$= \left[1 + \left(\frac{\frac{1}{2}\sum_i^n |\nabla\Psi_i|^2 - \frac{1}{8}\frac{(\nabla\rho_\alpha)^2}{\rho_\alpha} - \frac{1}{8}\frac{(\nabla\rho_\beta)^2}{\rho_\beta}}{2^{2/3}C_F(\rho_\alpha^{5/3} + \rho_\beta^{5/3})}\right)^2\right]^{-1}$$

$$C_F = \frac{3}{10}(3\pi^2)^{2/3} \tag{7}$$

where ρ_α, and ρ_β denote the spin densities; C_F is the Fermi constant; $t_{P,\alpha}$ and $t_{P,\beta}$ are the spin-dependent parts of the kinetic energy density for the system; $t_{h,\alpha}$ and $t_{h,\beta}$, similarly, represent the kinetic energy density of the spin-polarized homogeneous electron gas. The ELF values are bound between 0 (low localization) and 1 (high localization). We have determined the spin-polarized average of ELF (plotted in Figure 11). We have also examined the separate spin-α and spin-β orbital contributions. Along the reaction pathway ELF varies parametrically with the nuclear configuration, and the transformations in bonding are manifested in the appearance and disappearance of local maxima. Figure 11 depicts these transformations in ELF. In the top two panels of Figure 11 we have shown configurations, in which the mobile proton H resides on the oxygen atom of the metal-bridging water molecule. The electron localization function plot indicates pronounced hydrogen bonding, exemplified by the presence of a region between the H and the O′ atom of Asp128, where ELF takes values close to 0.5 (electron localization comparable to the case of uniform electron gas, shown in green). In the next panel we observe the initial

(40) Kohut M.; Savin A. *Int. J. Quantum Chem.* **1996**, *60*, 875−882.
(41) Silvi, B.; Savin, A. *Nature* **1994**, *371*, 683−686.
(42) Becke, A. D.; Edgecombe, K. E. *J. Chem. Phys.* **1990**, *92*, 5397−5403.
(43) The ELF homepage at http://www.cpfs.mpg.de/ELF

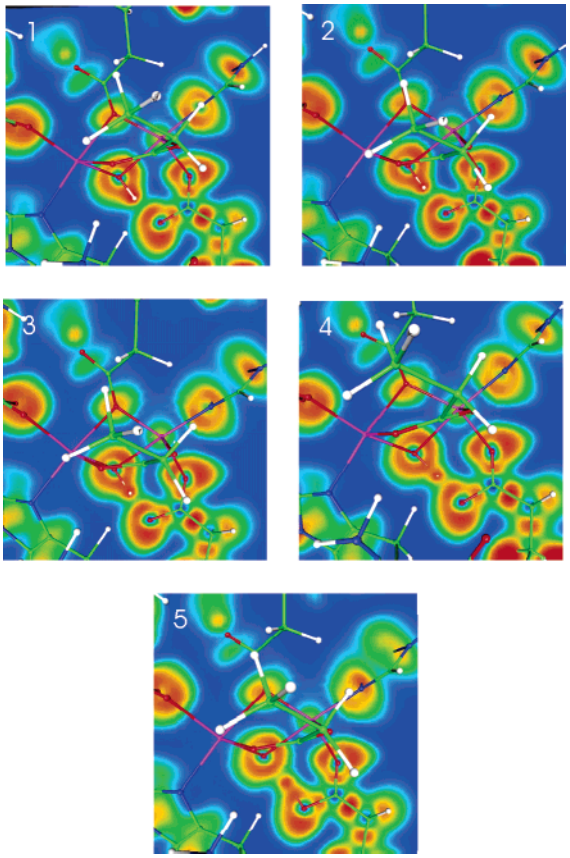

Figure 11. Contour plots (1−5) of the electron localization function (ELF) for five snapshots taken from the AIMD trajectory during a proton-transfer event.

elongation of the O*−H bond and the concomitant elongation of the corresponding basin of attraction in ELF. The following panel represents a configuration selected to be closest to the transition state for the deprotonation process. By the presence of two distinct basins of attraction corresponding to the O*−H bond and the O′−C bond of Asp128, we infer the transition state has not been reached yet. However, we see the formation of a neck region in the ELF density between the O* atom and the H atom, which seems to migrate by forming its own basin of attraction. From this we conclude that the deprotonation process has a partially covalent character. Furthermore, the increase in the ELF density between H and O′ (indicated by yellow color) signifies that the formation of a covalent bond between them has already begun. The final panel in Figure 11 depicts a configuration immediately following the migration of the mobile proton. It shows that the basin of attraction for the H atom has merged with the basin representing the O′ atom of Asp128. In general, we conclude that the electron localization function is very useful in following the bond transformations in our system and provides insight into the microscopic mechanism of the deprotonation process.

4. Concluding Remarks

Ab initio molecular dynamics has provided in recent years unprecedented insight into condensed phase processes. However, applications to transition metal systems and, in particular, enzymes still present major challenges. We have carried out computationally demanding ab initio molecular dynamics calculations on models of the active site of rat liver arginase. The obtained structural results are in good agreement with the available experimental data. Moreover, our calculations provide interesting new dynamic and energetic details to complement the structural data. The Asp128 residue was identified as a likely deprotonating group for the bridging nucleophile based on the formation of a strong short hydrogen bond, which is preserved even in the metal-depleted form. This fact may explain the partial activity of the metal-deficient form of the enzyme. Electronic structure analysis from a previous study revealed that orbitals involving the terminal Asp234 and the bridging Asp232 lie at high energies, suggesting them as potential departing ligands in agreement with recent experimental findings. This is indeed what we observe in the course of our direct dynamics trajectories, demonstrating a labile coordination for these residues and carboxylate shifts in the case of Asp234. Additionally, our constrained dynamics results implicate Asp232 as a departing ligand in the observed proton transfer to Asp128. Direct AIMD simulation revealed low barrier proton transfer events from the bridging water molecule to the catalytically essential Asp128 residue in accord with conclusions from a recent biomimetic study.[12] No proton transfer was observed in the case of metal-depleted arginase. Our calculations provide a detailed picture of the chemical and hydrogen bonding in the active site that can serve as a basis for further inquiry into the mechanism of catalytic action in arginase. Our results clearly demonstrate that first principles molecular dynamics calculations on realistic models of enzymatic active sites are now possible. Future work will examine applications of the Car−Parrinello methodology and novel methods for finding reaction paths[44,45] to the study of the catalytic activity of arginase and, more specifically, the initial nucleophilic attack in the first step of the catalytic cycle.

Acknowledgment. We thank Prof. David Christianson and Dr. Evis Cama for helpful discussions and for sharing preliminary results with us. We also thank Dr. Petra Munih, Dr. Robert Doerksen, and Dr. Alessandra Magistrato for their thoughtful comments on this work. Generous financial support from the National Science Foundation and the National Institutes of Health is gratefully acknowledged. Computer resources were provided, in part, by the Pittsburgh Supercomputing Center through NPACI.

JA043693I

(44) Bolhuis, P. G.; Chandler, D.; Dellago, C.; Geissler, P. L. *Annu. Rev. Phys. Chem.* **2002**, *53*, 291−318;
(45) Laio, A.; Parrinello, M. *Proc. Natl. Acad. Sci. U.S.A.* **2002**, *99*, 12562−12566.